CHAPTER 2 LITERATURE SURVEY

Two approaches are discussed to highlight the complex nature of the AG/SAG mill modelling when applying Population Balance Modelling. The DEM, which is a viable alternative for SAG modelling is discussed in detail. The information from the DEM has to be complemented by the material fracture response data. Thus fracture is also discussed to some considerable detail.

2.1 Steady state mill simulations

The milling process can be described as a reactor process that involves the conversion of a coarse feed into a finer product. For this to happen, a series of fracture events must take place within the mill. The overall rate of this process is a function of the forces prevailing within the mill and the physical properties of the material involved.

Two functions are used to define the process; the propensity for breakage (selection function) and the characteristic distribution of the fragments (breakage distribution function). Using these functions, the mass balance for material within a discrete fraction of size class i can be written as follows.

Rate of production of size i	=	Rate of new feed of size i entering the system	+	Rate of larger sizes breaking into fraction i	-	Rate of size i breaking into smaller sizes

This can be expressed in matrix form as follows:

$$Fp_i = Ff_i + W\left(\sum_{j=1}^{i-1} b_{ij} S_j w_j - S_i w_i\right) \qquad i = 1,2....n \qquad (2.1)$$

where p_i, f_i and w_i are the respective product, feed and mill content fractions of the size class *i*. S_i is the breakage rate or selection function and b_{ij} represents the fraction that appears in class *i* from breakage occurring in class *j*. F is mass flow rate of the feed and W the mill hold-up of the ore.

This equation forms the basic building block used for simulating grinding. It has already been mentioned that this approach has been remarkably successful with ball mill simulation while for AG and SAG mills it is still attended by some difficulties. Significant progress in the development of the models for SAG and AG mill simulations have been made by the JKMRC (Leung 1987, Napier-Munn et al 1996) , Austin et al (1987) and Herbst et al (1993). These are probably the most well known methods and are briefly reviewed.

2.2 The JKMRC model

The model builds on equation 2 but with some modification based on two assumptions; the system is at steady state and hence there is no net accumulation, secondly, material within the mill is perfectly mixed and thus the discharge content is representative of what is inside the mill. In view of these assumptions the following equations are derived:

$$0 = f_i - d_i s_i + \sum_{j=1}^{i-1} r_j s_j a_{ij} - r_i s_i \qquad i = 1,2....n \tag{2.2}$$

$$d_i s_i = p_i \tag{2.3}$$

for size class *i*, d_i the discharge rate (fraction of the mill content that is discharged per unit time), a_{ij} like b_{ij} is the fraction appearing in interval i after breakage in interval j. r_i is the breakage rate and s_i the fractional content of size interval i.

2.2.1 Discharge rate

The discharge rate comprises the transportation model and the classification model and is stated as follows:

$$d_i = d_{\max} \times C_i \qquad (2.4)$$

where for size *i*, d_i is the discharge rate, C_i the classification function and d_{max} is the fraction of the load presented to the grate per unit time. The classification function is a dimensionless value between 0 and 1 and is related to size by a well defined relationship (Napier-Munn et al 1996). The d_{max} is in some way related to feed rate, feed size distribution and mill fill level in a complex way and is discussed elsewhere in greater detail (Leung 1987, Austin and Barahona, 1986, Austin et al 1976). The basic equations are given below.

$d_{\max}$ falls on the L operating curve (Leung 1987) (2.5)

$$L \text{ defined as } \frac{volume\ of\ subgrate\ size}{volume\ of\ mill\ content} = m_1\left(\frac{Feed\ volume}{Active\ mill\ volume}\right)^{m_2} \qquad (2.6)$$

For the Leung model m_1 and m_2 are both assumed as 0.37 and the required d_{max} value is iterated to obtain a solution that satisfies both Equations (2.4) and (2.6). This assumption ignores the effect of feed size distribution (Duckworth and Lynch 1982) and the increase in fines production when abrasion dominates with higher mill fillings. The effect of viscosity is also not considered.

For this reason a more robust model that relates slurry hold-up to grate design, grate open area and mill speed was introduced in the variable rate model and is discussed by Morrell and Morrison (1996). It is stated as follows:

$$J_p = kQ^{0.5}\gamma^{-1.25}A^{-0.5}\Phi^{0.67}D^{10.25} \qquad (2.7)$$

where

Jp = fractional slurry hold-up

k is a constant

Q = volumetric flowrate out of the mill (m^3/hr)

γ = mean relative radial position of the grate apertures

A = total area of the grate arpertures (m^2)

ϕ = fraction of critical speed

D = mill diameter (m)

The mean relative radial position of the grate apertures can be calculated as follows:

$$\gamma = \frac{\sum r_i a_i}{r_m \sum a_i} \qquad (2.8)$$

where

a_i = open area of all holes at radial position r_i

r_m = radius of mill inside the liners

Although this approach is a great improvement over the Leung model, it still does not address the effect of grinding mechanism on material transportation. In this equation, it is still assumed that high flow rate out of the mill will always correspond to a greater hold-up in the mill. There are however indications that in some cases a high load in an AG mill enhance the abrasion mechanism which results in finer product but lower throughput (De Beer et al 1997)

It must be added that the transportation models have continuously undergone revision and more recent updates of the models are discussed in Apelt's PhD thesis (2002)

2.2.2 Breakage

The breakage inside the mill is described by the selection and the breakage distribution functions which are determined by elaborate laboratory procedures.

2.2.2.1 Determination of the Breakage distribution functions

Single particles within different size classes are broken by impact at carefully calculated energy inputs using the drop weight tester described in Chapter 4. The fraction of material broken below $1/10^{th}$ of the original size, referred to as t_{10}, is the basis for defining a relationship between the specific input energy and the breakage characteristics of an ore and is stated as follows:

$$t_{10} = A(1 - e^{-b.Ecs}) \qquad (2.9)$$

Ecs is the specific comminution energy (Kwh/t), while A and b are impact breakage parameters that characterise the ore. The t_{10} value can be converted to the breakage distribution function by applying appropriate equations (Leung 1987 and King and Bourgeois 1993).

The model has been criticised for ignoring the size effect. Yet as seen from the data presented in Chapter 4, it is of great significance. Banini's work (2001) also shows that particle size has an effect on the t_{10} values. In more recent JKRMC papers a modified equation shown below is used (Alpet 2002, Valery Jnr 1998).

$$t_{10_i} = A(1 - e^{-b.Ecsi}) \qquad (2.10)$$

The t_{10} described above represents breakage resulting from impact only. This value has to be combined with another value t_a related to abrasion. The method for obtaining the t_a value is discussed in the JKRMC Handbook (Napier-Munn et al 1996). The final t_{10} value is thus a weighted combination of the t_{10}-impact and t_{10}-abrasion.

The expected Breakage distribution function of each size fraction in the mill is related to the assumed energy input that the size fraction receives. As purely a matter of convention the highest energy level (E_1) which is based on the highest possible potential energy, is assumed to be targeting the coarsest fraction in the

mill. Corresponding lower energy levels E_i are calculated and assigned sequentially to lower size fractions.

E_1 is calculated from the potential energy of the geometric mean of the top 20% fraction size of the load (denoted as S_{20}) at full height in the mill and is calculated as follows:

$$S_{20} = (p_{100} * p_{98} * p_{96} \cdots p_{80})^{1/11} \qquad (2.11a)$$

$$E_1 = \frac{4}{3}\pi (S_{20})^3 \rho_{ore} gD \qquad (2.11b)$$

where ρ_{ore} is the ore density, g is the gravitational acceleration and D the mill diameter.

For a mill that also contains steel media, the steel balls are resized to ore sizes of equivalent mass.

The lower energy levels are derived using the equation below.

$$E_i = E_1 \left(\frac{x_i}{x_1} \right)^{1.5} \qquad (2.12)$$

where x stands for the screen fraction size.

Using this equation, the t_{10} value for each size fraction is obtained and by referring to an existing JKMRC database the Breakage distribution function of the sample is estimated.

2.2.2.2 The selection function.

This is defined by a set of spline curves that pass through five nodes at selected particle sizes. The values at these nodes have been determined experimentally and span a wide range of milling conditions.

2.2.3 Conclusion

While the value of the JKMRC simulation models are recognised internationally, the heavy reliance on the database is a serious disadvantage to independent modellers who do not have access to these data. It also limits the modellers to conventional cases and leaves little room for novel designs

2.3 The Austin Model

Austin has made a great contribution to the development of the selection and Breakage distribution function concept in the last forty years and is an author and co-author of books and many papers on the subject (Gardner and Austin 1962, Austin 1972, Austin et al 1984). The models have been a success for ball milling simulation. To extend the concepts developed for ball milling to (S)AG milling, he had to treat two size ranges differently; the above grate and the sub-grate size fraction. He identified three size reduction mechanisms; chipping, abrasion and disintegrative fracture which had to be modelled.

2.3.1 General model structure

The representation in the diagram below identifies the terms that are manipulated to establish the PBM equations - Fully mixed assumption.

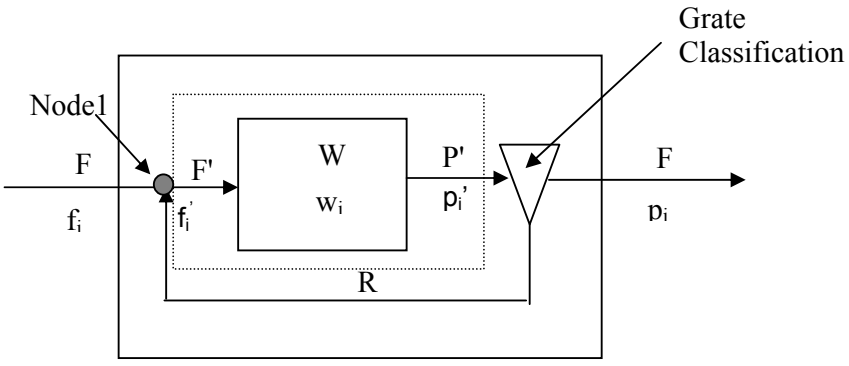

F = new feed, F' = new feed + recycle, P = Product, R = Recycle,
W = mill content. P' = product before grate classification

Figure 2-1Illustration of the model set-up for Autogenous mill simulation

The uppercase symbols represent tonnage flow. The lowercase symbols subscripted by i represent the fraction of the i^{th} range in each of the streams.

As in the JKMRC model, the grate is considered as an internal classifier which retains all the above grate-size material and a fraction of the sub-grate sizes. The internal classification function C' is defined as the ratio between mass of recycled material and mass of material that leaves the mill. Precise ways of estimating the entire classification vector values are discussed elsewhere (Austin et al 1986).

The mass balance at node 1 in Figure 2.1 can be written as follows:

$$F' = F + R \quad = F + FC' \quad = F(1 + C') \tag{2.13}$$

where C' is the ratio of mass of material retained to that discharged.

The mill hold-up τ is equal to the mill load divided by the feed rate (W/F), similarly τ' is defined as follows:

$$\tau' = {}^{W}\!/_{F'} \quad \therefore \quad \tau = \tau'(1 + C') \tag{2.14}$$

W may be calculated from the load cell readings or by weighing the load when the mill is stopped and the charge dumped. Austin has proposed a theoretical method for estimating τ (Austin et al 1987).

Equation 2.1 can be re-written in terms of τ as follows:

$$p_i = f_i + \tau\left(\sum_{j=1}^{i-1} b_{ij} S_j w_j - S_i w_i\right) \tag{2.15}$$

An expression for the mass balance at the grate classifier can be written as follows:

$$P = \sum P' w_i (1 - c_i) \quad = \sum F' w_i (1 - c_i) \tag{2.16}$$

Since P = F and F' can be replaced by the term (1+C') F; these can be substituted into Equation 2.16 to yield the following equation:

$$1 + C' = \frac{1}{\sum w_i (1 - c_i)} \tag{2.17}$$

Applying Equation 2.15 to the system using $w_i = p_i'$ yields the following equation:

$$w_i = \frac{f_i + \tau \sum_{j=1}^{i-1} b_{ij} S_j w_j}{(1 - c_i)(1 + C') + \tau S_i} \tag{2.18}$$

The equations above consider breakage by fracture disintegration only, to include abrasion and chipping a more complex treatment is required (Menacho 1986, Austin et al 1987). A successful simulation using the equations above is presented by Amestica et al (1993). In this particular case the hold-up is estimated from mill power.

2.3.2 Determination of the breakage distribution and selection functions.

2.3.2.1 The selection function

This involves a separate treatment of the two size fractions; the coarse size which is too strong to sustain fracture under the action of available media and the fine which can be nipped and broken. For the fine size, the equations that have been developed for the ball mill are applicable with the provision made to cater for the lower density of the ore media in comparison to steel balls (Austin et al 1987). The media ore shape aspect is not considered. The standard methods of

determining the selection and breakage functions with the prescribed correction factors for a range of conditions are well documented in the (Austin et al 1984) text.

For the coarser material breakage is assumed to be a combination of chipping, abrasion and self-breakage. The term self-breakage is used loosely and refers to breakage that occurs when a falling big rock breaks due its own weight.

When a rock just enters the mill, chipping is dominant as the sharp and rough edges get subjected to higher levels of stress than the rest of the body. The removal of these edges produces fragments that are coarser than the fine powdery product of abrasion. Once the rock is well-rounded, wear thereafter progresses by abrasion. The wear laws developed for the steel media in ball mills (Austin and Klimpel 1985) have also been found to describe well the wear of the ore media.

The likelihood of self-breakage is assumed to increase with increasing lumps size. Thus the resulting selection function curve indicates the lowest rates for particles that can neither be nipped efficiently nor are big enough to fracture by self-breakage. The resulting plot of selection function is typically as shown below:

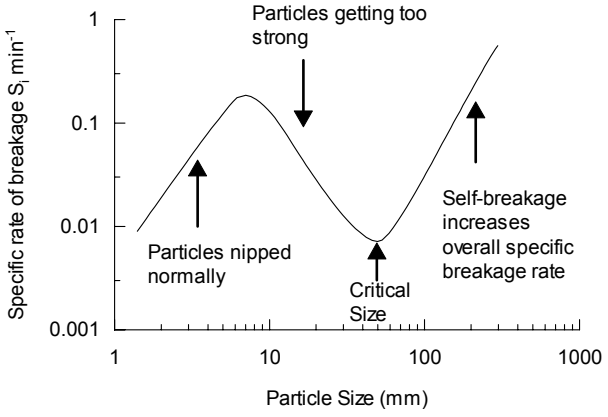

Figure 2-2 The changing Specific Breakage rates with particle size

The overall selection function is thus a combination of these factors, namely; breakage by nipping of the smaller particles and chipping/abrasion and self-

breakage of the larger rocks. The implementation of these equations is a considerable challenge and is dealt with in the relevant papers (Menacho 1986, Austin et al 1987).

2.3.2.2 The breakage distribution function

The determination of this function involves determining the suitable weighting values for each of the breakage mechanisms discussed above. The equations and the required parameters are discussed extensively by Austin and Tangsriponkul (1994). It is apparent that considerable effort is required in taking the necessary measurements and the method still requires more tests for validation.

The mechanistic approach of the models is obviously advantageous, however the authors of these models admit that further work is required to adequately describe the complex AG/SAG grinding process (Austin et al 1987).

2.4 Herbst dynamic simulator

Herbst's approach to Population Balance Modelling differs from the other two in one respect, the selection function is linked to the specific power input (Herbst and Fuerstenau 1973, 1980). Thus the scale-up from the standard test mill to any other mill will be related to the specific power. A fairly comprehensive procedure that applies specific power selection function is given by Sepulveda (2001).

The current models that are available in the Min00cad simulation package for both ball and SAG developed by Herbst, go further by including the liberation model (Herbst et al 1993). Instead of assuming steady state, the hold-up can accumulate mass and thus will dynamically respond to circuit disturbances.

The use of specific power assumes that the mechanisms in the test-mill and large mill will remain the same. This weakness has been recognised and in the latest edition the specific breakage rates can be adjusted according to the mill environment (Herbst and Pate 2001). By use of the High Fidelity Simulation

(HFS) DEM Software, the estimation of selection function parameters for the Min00cad simulator is greatly improved (Herbst and Nordell 2001).

2.5 The Discrete Element Method

This technique is relatively new and has been helped by the availability of high-power computers. Following the pioneering work of Cundall (1971, Cundall and Strack 1979), Mishra and Rajamani (1990) saw the potential of extending this technique to grinding. The potential of applying this technique to the minerals industry in general is vast as particles are encountered in many unit operations.

The DEM involves the application of Newton's laws to describe the motion of particles and the implementation of a surface response procedure when a collision occurs. The soft contact approach proposed by Cundall allows an overlap to occur between two approaching entities. The contact force then is a function of the overlap distance and the stiffness of the material. The implementation of these equations in a system of interacting particles each with a complex boundary is very demanding computationally.

There are four main parts that comprise the DEM:

- Object representation
- Contact detection
- Contact resolution
- Motion physics

2.5.1 Object representation

The simulation involves both moving and non-moving elements that interact at their boundaries. For a mill, solid lines or planes with adjoining nodes are used to

represent the internal geometry. The movement of the mill wall is determined by the initial speed and does not in any way react to collisions.
The particles are usually represented by discs or spheres in most minerals engineering applications. The unique properties of a circle or a sphere make the algorithms such as contact detection easier to handle. This kind of shape representation works well for balls in ball mills, however for ore particles with arbitrary shape this may result in inaccurate dynamic behaviour. For example spheres would be unsuitable for simulating formation of a conical pile on a flat surface. For this reason ways of implementing non-spherical shapes have also received much attention as seen in the on-going effort discussed below.

2.5.1.1 Methods used to represent arbitrary shapes

Use of ellipses

Rounded ore particles tend to be more ellipsoidal and can thus be represented by ellipses in 2D or ellipsoids in 3D. Ting with his collaborators has developed a code that he claims to be efficient for handling ellipses in 2D simulations (Ting and Corkum 1992).

Use of Superquadrics

Two-parameter Superquadric equations (Barr 1981) have also been suggested as a way of representing a very wide range of shapes with smooth surfaces. In spite of their flexibility, precise resolution of the contact is usually computationally expensive.

Use of the Discrete Function Representation

Williams and O'Connor (1995) who applies what he calls the Discrete Function Representation (DFR) claims that this method is superior to continuous functions for arbitrary shape representation. This involves using discrete wall boundaries in place of continuous functions. Minimising the discrete wall number that define a shape is essential for limiting computational expense. Not much documentation is available elsewhere to confirm the effectiveness of this approach.

Use of bonded spheres

Some modellers have opted to retain the spheres or discs and bond these to represent more complex shapes (Favier et al 1999). This unfortunately introduces extra computation overheads as the list of all the spheres/discs that make the agglomerated particle must be maintained. This scheme is also available in the DEM software engine that was used to develop the simulator for this research.

Finding the most effective way of representing the shapes of simulated particles still remains an active research topic. For this project the use of spheres and discs was retained.

2.5.2 Contact detection

The main purpose of this scheme is to identify the elements that are in contact. Using straight -forward checking schemes would require at least $(n^2 - n)/2$ tests (when duplication is avoided) for n particles (Misra and Cheung 1999). It can be seen that the increase in time required for the completion of a contact detection routine increases by a square for every particle added. For a large number of particles this is a considerable computational expense and thus various schemes of managing this problem more efficiently have been proposed. One method which works well is the spatial sorting technique. Particles are pre-sorted so that collision checks are limited to only particles which are likely to collide (i.e. close neighbours).

A technique that has been employed in the Utah Millsoft Program involves dividing the simulation area into grids. The centres of the particle(s) or wall line(s) are linked to the cells in which there are found. The grid size is determined such that search for possible contacts is limited to immediate neighbouring grid cells (grid resolution is equal to the diameter of the largest particle). Apart from the extra book keeping for the grid data, the computation costs for every extra particle added only increases linearly (Mishra 1991).

The contact detection is the most expensive part of the computation and thus also remains an active area of research.

2.5.3 Contact resolution

The main purpose of this procedure is to resolve the extent of overlap occurring between two elements so as to enable the interaction forces to be calculated. The determination of the overlap is easiest between discs or spheres. For more complex shapes, bounding squares or circles are used for a quick check of a possible contact before employing a more detailed analysis of the contact (Williams and O'Connor, 1995).

The calculation of the forces below is shown for the simplest case involving discs. This procedure is also applicable to particles of arbitrary shape provided the directions of the tangential and the normal forces have been determined.

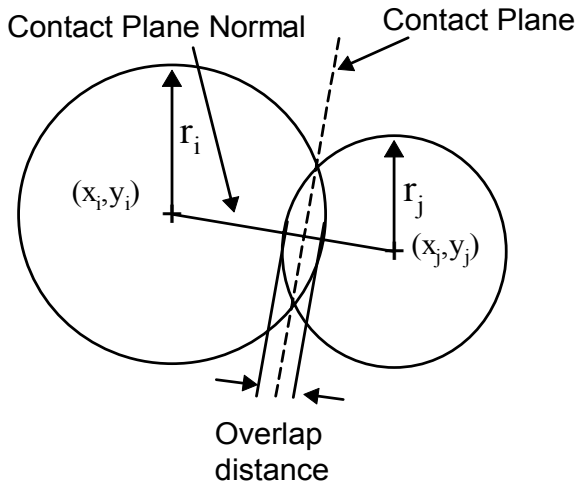

Figure 2-3 Illustration of a ball to ball contact

It can be seen that the overlap distance (Δ_n) for the purpose of determining the normal force is:

$$\Delta_n = r_j + r_i - \sqrt{\left(x_j - x_i\right)^2 + \left(y_j - y_i\right)^2} \qquad (2.19)$$

where r represents the radii of the elements i and j, x and y being the Cartesian positions of their centres.
Determining the overlap between a disc and the wall is more problematic as contact can occur with the edge or the corner (end of two walls) or the corner and the edge at the same time. This problem has been addressed by several authors (Cundall 1988, Mishra 1991, Hogue 1993).

Once the overlap has been determined for two elements in contact, the prevailing forces (normal, shear and angular) at the point of contact can then be calculated. The normal force is modelled as visco-elastic, *i.e.* it consists of an elastic (spring) and a viscous damping (dashpot) component. The force in the tangential direction (shear), includes a slider in addition, to model friction. The following equations represent the contact forces.

$$F_n = K_n \Delta_n + C V_n \tag{2.20}$$

$F_s = K_s \Delta_s + C V_s$ when $F_s \leq \mu F_n$ otherwise sliding is implemented instead and then $F_s = \mu F_n$ (2.21)

where F is the force, K is the stiffness, Δ is the change in overlap and V the relative velocity at the point of contact. Normal and Shear directions are denoted by the subscripts n and s.

There are some problems that are associated with the linear spring and dashpot model which are discussed in Chapter 6.

2.5.4 Motion physics

The resultant forces based on calculations in section 2.4.3 are then applied to the affected particles to compute linear and angular acceleration as in the equations below.

$$F_i = m\ddot{x}_i \qquad i = x,y \text{ for 2D simulation or } x,y,z \text{ for 3D} \quad (2.22)$$

where F is the force acting in the directions specified by i, and $\ddot{x}$ the corresponding acceleration, and m is the mass.

$$T = I\ddot{\theta} \quad (2.23)$$

where T is the torque, I is the moment of inertia and θ is the angular position.

The velocity and the displacement are computed by successive numerical integration of the acceleration. The resulting particle positions are also updated by adding the displacements to previous positions.

2.5.5 Conclusion

The attractiveness of the DEM is its reliance on fundamental laws to predict the behaviour of particulate systems. In particular, interparticle forces and energy dissipations are predicted – important variables used in the description of particle fracture. It is however clear from this review that many areas of the DEM code remains matters for further research. A user needs to be aware of these limitations when planning to use this code.

2.6 Contact mechanics

The DEM model concerns itself with the dynamics of particles and the energy conversions that occur as particles interact. However for the purpose of predicting

breakage rate in a mill the nature of stress applied and its effect on particles also requires attention.

2.6.1 Conditions necessary for fracture

The main aim of this review is to establish whether it is possible to predict the fracture of a particle of any size when the energy input is known, from theory.

2.6.1.1 General elastic theory

From elastic theory it is known that most particles under stress undergo deformation in proportion to the applied stress as long as the deformation is elastic. This proportionality law is only obeyed up to a limit, beyond which the body may experience plastic deformation or breakage. Brittle particles fail without experiencing much plastic deformation prior to breakage.

If the highest force attained before a brittle solid breaks is known, the energy input required for breakage can be calculated by integrating the force over the distance of elastic extension. The equation for a cubic element of dimension Δx, Δy and Δz stretched in the z direction by a force F is written as follows:

$$\Delta U = \left(\frac{1}{2}\Delta F\right)\varepsilon\Delta z \qquad (2.24)$$

where ΔU is the energy input and $\varepsilon\Delta z$ is the elastic extension. Since the force increases linearly from zero to the final magnitude, the average force is therefore $\frac{1}{2}\Delta F$. This can be expressed in terms of stress as follows:

$$\Delta U = \left(\frac{1}{2}\sigma\Delta x\Delta y\right)\varepsilon\Delta z \qquad \sigma \text{ being } Force/Area \qquad (2.25)$$

The energy stored per unit volume $\Delta U/\Delta V$ (strain energy density), because $\Delta V = \Delta x.\Delta y.\Delta z$ is therefore:

$$u = \frac{1}{2}\sigma\varepsilon \qquad \text{Where } u = \frac{\Delta U}{\Delta V} \qquad (2.26)$$

Applying Hooke's law which states that $\sigma = Y\varepsilon$ (where Y is the modulus of elasticity), the equation becomes:

$$u = \frac{1}{2Y}\sigma^2 \qquad (2.27)$$

Thus the total strain energy that any solid can store before fracture or plastic deformation occurs can be obtained by multiplying Equation 2.27 by its volume. The prediction of particle failure from the consideration of elastic theory apparently looks easy; however the nature of particle loading and effect of internal particle defects also requires attention.

2.6.1.2 The distribution of stress in a particle under stress

Oka and Majima (1970) have done experiments to show the pattern of stress that develops when an elastic sphere is compressed between two plates. Two cones of high local stress develop in the sphere at the points in direct contact with the plates. The cones tend to act as wedges that try to split the sphere as shown. It can be seen that some tensile stress develops in the direction perpendicular to the applied stress. This stress pattern was repeated in a cube and in an irregularly shaped particle.

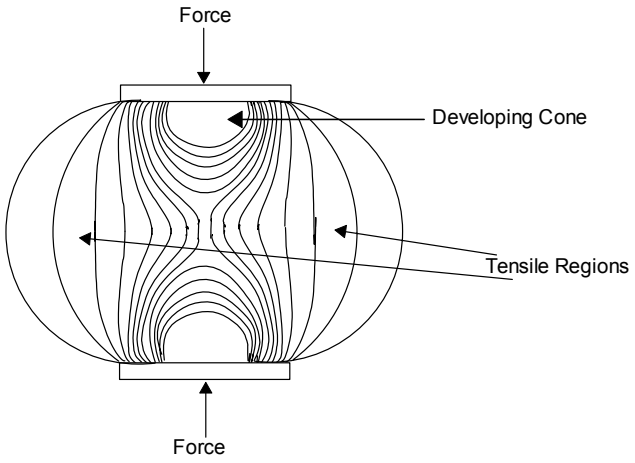

Figure 2-4 Stress pattern developed under compression

The complex stress pattern that develops illustrates how prediction of particle failure can become a complicated issue. More importantly, the stress pattern that develops gives an indication of the particle size distribution that would result if stress were to be increased to fracture point. Coarse fragments would emerge from the mostly tensile stressed regions and fines from regions immediately below the loading plates which are in a state of compression. The bimodal size distribution that is typical of crusher product is a consequence of this phenomenon (Prasher 1987).

Gorham and Salman (1998) who have done a lot of high speed impacts by projecting spheres against a stationary surface observed that speed i.e. stress rate had an influence on the breakage pattern. The likelihood of breakage could also be correlated to the energy input.

2.6.1.3 The distribution of stress around cracks

The stress pattern that develops in a stressed particle is further complicated by the presence of flaws. These act as stress concentrators. A 2D analysis of a uni-axially tensile loaded thin plate with a known crack length is illustrated below.

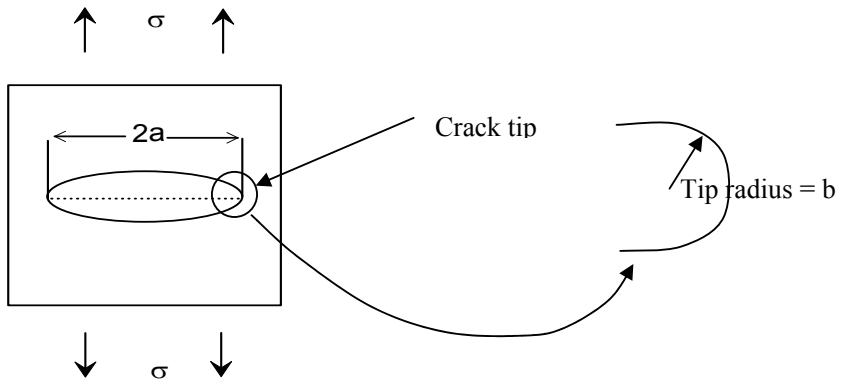

Figure 2-5 Application of stress perpendicular to the crack

The applied stress σ tends to "concentrate" at the tips of the crack and the solution for crack tip stress derived by Inglis (1913) is given as:

$$\sigma_T = \sigma\left(1 + 2\sqrt{\frac{a}{b}}\right) \qquad (2.28)$$

where a is the half-length of the crack and b is the radius of the tip. σ_T is the stress at the tip and σ is the applied stress and $\left(1 + 2\sqrt{\frac{a}{b}}\right)$ is the so called "stress concentration factor". It follows that as b tends to zero the stress at the tip tends to infinity. However this never happens as the application of any force normal to the crack will always deform it and hence b will always have a value greater than zero.

2.6.1.4 The energy requirements for crack propagation

Using Equation 2.28 the stress that develops at the crack tips can be calculated and the probability of atomic/molecular bonds rupturing evaluated. However for the process of crack propagation to proceed, sufficient energy must be available for the creation of two new surfaces. Griffith's theory (1924) is on hand to analyse conditions for unstable crack propagation.

The total energy of a cracked body under stress can be written as follows:

$$U_T = W + U_c - U_e - U_s - U_x \qquad (2.29)$$

U_T is the total energy of the system
W is the energy input to the system
U_c is the energy released within the body when the strain energy is relaxed by crack extension
U_e is the strain elastic energy accumulated by a stressed body
U_s is the energy absorbed into creation of new surface
U_x accounts for many other energy changes that cannot be measured as discussed by Rumpf (1973) (i.e noise, heat, etc.)

For the analysis of the energy balance equation above the terms must be expressed using elastic equations.

The strain energy is obtained by multiplying the volume of the plate with the strain energy density derived in Equation 2.27. When the plate thickness is assumed as unity, strain energy is then expressed as follows:

$$U_e = \frac{1}{2Y}\sigma^2 A \tag{2.30}$$

Where A is the area of the plate

The energy released is derived by considering the crack surface displacement in the x,y direction which is based on Muskelishvili's (1953) solution for the displacements and is given as:

$$U_c = \frac{\pi\sigma^2 a^2}{2Y} \tag{2.31}$$

The surface energy which is due to the upper and lower crack surface areas and the specific surface energy, is as follows:

$$\mathrm{U_s} = 2(2\mathrm{a})\gamma_\mathrm{s} = 4\mathrm{a}\gamma_\mathrm{s} \tag{2.32}$$

Equation 2.29 can then be re-written with the terms substituted as follows:

$$U_T = \frac{1}{2Y}\sigma\varepsilon + \frac{\pi\sigma^2 a^2}{2Y} - \frac{1}{2Y}\sigma^2 A - 4a\gamma_s - U_x \tag{2.33}$$

From the equation above it is seen that for any increase in crack length the energy released increases by a square law while the energy consumed by new surface creation increases linearly. Thus a point is reached when the energy release rate

exceeds that which is consumed and unstable crack propagation results. When this point is reached external energy input is no longer required to sustain crack propagation.

If U_x is ignored then the critical point is when U_c (energy released) is just equal to U_s (surface energy).

$$\frac{\pi\sigma^2 a^2}{2Y} = 4a\gamma_s \tag{2.34}$$

This leads to:

$$\sigma = \sqrt{\frac{2Y\gamma_s}{\pi a}} \tag{2.35}$$

This analysis lays the foundation of modern linear elastic fracture mechanics (LEFM). It is however necessary to appreciate other complicating factors such as plastic deformation and micro-cracking around the crack region. In the above analysis, the crack is assumed to be perpendicular to the direction of stress application while in real life crack orientation can be in any direction and thus complicating the analysis further.

In spite of the developments in fracture theory, prediction of the probability of failure from fundamental theory remains intractable. In most cases a statistical approach is preferable or has to be combined with the analytical approach. One such approach is the model proposed by Weibull (1951) which is briefly discussed.

2.6.1.5 A statistical model for predicting particle failure

A model which predicts the likelihood of encountering a critical defect in a particle of some relative size has been proposed by Weibull (op cit). A random distribution of flaws in terms of size and orientation with a consistent density is assumed for a given sample of specimens. The chances of finding a critical flaw

increases with the size or length of the specimen. If the probability of failure for a single component *s* of a specimen is P_f when stress σ is applied, the chance of survival P_i is then equal to $1\text{-}P_f$. For a sample comprising *n* of *s* components for which failure of any of the components constitutes overall failure, the probability of survival of the system is the product of the survival probabilities of all the parts and is written as follows (Carter 1972):

$$R_s = \prod_{i=1}^{n} P_i \tag{2.36}$$

The probability of survival of the system decreases exponentially with the increase in *n* components and can be re-written as follows:

$$R_s = e^{-P_i n} \tag{2.37}$$

The probability of failure R_f of the system is simply $1\text{-}R_s$ and can be written as:

$$R_f = 1 - e^{-P_i n} \tag{2.38}$$

To determine P_f Weibull proposed a defect density distribution termed the Weibull distribution which is expressed as follows:

$$\mathrm{P_f} = \int_0^{\sigma} \mathrm{g}(\sigma)\mathrm{d}\sigma = \left[\frac{\sigma - \sigma_l}{\sigma_0}\right]^{\mathrm{m}} \tag{2.39}$$

where σ_l is the lower limit to the strength, m is the Weibull modulus and σ_0 is the scale parameter.

These parameters can be substituted into Equation 2.38 to yield the following equation:

$$R_f = 1 - e^{-\left[\frac{\sigma-\sigma_l}{\sigma_0}\right]^m n} \quad (2.40)$$

The parameters can be derived experimentally for any particular material (usually brittle) under study.

2.6.1.6 Conclusion

It is possible to get to some distance with the theoretical analysis of conditions that may lead to fracture. However the presence of flaws and variation in the mode of stress application makes the analysis too complex and generally only statistical trends can be established.

From Weibull's analysis it is apparent that purely due to the natural distribution of flaws in materials, an increase in specimen size increases the probability of failure. Thus for the same material a larger particle is expected to be relatively weaker than a smaller one.

2.6.2 Product size distribution

So far conditions that may lead to a particle breaking have been explored. In minerals engineering as already discussed under the simulation models, the description of fragment distribution is also equally important.

From the theory discussed so far, three factors that would affect size distribution are identified as follows:

(a) Distribution of flaws; breakage is more likely to propagate along existing flaws than initiating new flaws.
(b) Number of contacting points; since points of contact in compression are sites of stress concentration, a particle in contact with many particles will break differently from that in contact with a few (Muller and Weichert 1990).

(c) Energy input; there must be sufficient energy for the crack propagation process. The availability of excess energy will also propagate cracks in the resulting fragments.

2.6.2.1 Effect of Distribution of flaws

Prior knowledge of the location of defects in particles is not possible. Thus the general approach is to establish the parameters of the Breakage distribution function from experimental data. Once these parameters have been established for a particular ore they are assumed applicable to all comminution situations.

2.6.2.2 Effect of Number of contacting points

Most of the studies on the effect of stressing particles under different stressing environments have been conducted by German researchers, particularly Schonert and associates (1990, 1994). The loading conditions studied were classified into four groups: single particle (free of interference from other particles), single particle layer, unconfined multi-particle layers and confined multi-particle layers under compression. The specific energy absorbed and progeny size distribution were affected by the particle arrangement and the initial size distribution. While this work is very promising there are still many possible configurations and materials yet to be studied.

2.6.2.3 Effect of Energy input

Using the JKMRC drop-weight tester and the Ultra-Fast-Load-Cell developed at Utah University it has been possible to study how energy input affects progeny size distribution. From the breakage of single particles, models have been developed to estimate the Breakage functions (Napier-Munn et al 1996, King and Bourgeios 1993).

2.7 Conclusion

Use of the DEM for simulating grinding is attractive as its approach is fundamental. However it is evident from the discussion of both the DEM model and fracture mechanics that while this approach tackles modelling at a higher

level of detail, aspects where simplification is an unavoidable compromise remain.